Exploration Geophysics (2000) 31, 134-139

EM-coupling removal from time-domain IP data

Peter K. Fullagar[1] Binzhong Zhou[2] Barry Bourne[3]

Key Words: Apparent resistivity, de-coupling, EM coupling, induced polarisation, inversion

ABSTRACT

Electromagnetic (EM) coupling of frequency-domain induced polarisation (IP) data has been the subject of many studies, and a number of 'de-coupling' procedures have been devised. However, there has been far less emphasis on coupling in the time domain, the normal approaches being to wait until late times and assume the EM contribution is insignificant or, less frequently, to invoke a Cole-Cole model to account for the EM-coupling response. A fast and simple procedure has been devised for suppression of EM-coupling effects in time-domain IP data. The essence of the approach is to represent the EM-coupling as a half-space decay. The half-space resistivity (EM apparent resistivity) is adjusted via inversion until the fit to the observed transient voltage decay is optimal in the least squares sense. The EM voltages associated with this best-fitting EM half-space decay are then subtracted from the measured voltages to yield a de-coupled 'IP transient'. Transients that are well represented by an EM half-space decay are deemed 'non-responsive' in the context of IP. Transients that deviate markedly from an EM half-space decay are indicative of high apparent chargeability. The application of the new procedure is illustrated on dipole-dipole IP data from the Yandal greenstone belt of Western Australia.

INTRODUCTION

There are two principal factors that restrict the sensitivity and usefulness of induced-polarisation (IP) measurements: telluric noise and electromagnetic (EM) coupling. Both telluric noise and EM coupling will cause IP-like effects that are not due to electrical polarisation. This paper describes a procedure for suppression of spurious EM effects in time-domain IP data.

EM coupling in frequency-domain IP has been the subject of a number of studies, many of which were inspired by a desire to perform spectral discrimination of IP sources, e.g., Hohmann (1973), Hallof (1974), Wynn and Zonge (1975), Pelton et al. (1978), Coggon (1984a,b), Song (1984), Grant (1990), Tripp et al. (1990). However, there has been far less emphasis on EM coupling in time-domain IP. Dey and Morrison (1973) published time-domain coupling curves for the dipole-dipole configuration over a homogeneous half-space and a suite of multi-layer cases. Trofimenkoff et al. (1982) derived late-time coupling formulae for dipole-dipole and Schlumberger configurations on a half-space, based on the exact expression for parallel wire coupling due to Yost (1952). More recently, Johnson (1990) modelled the measured voltage decay as a superposition of two Cole-Cole transients, one for the IP component and one for the EM-coupling component.

While 'de-coupling' is performed routinely on frequency-domain data, the time domain approach to coupling has generally been more cavalier: wait until late times and assume the EM contribution is insignificant. In this paper a simple algorithm for de-coupling of time-domain IP is described. The procedure has been implemented for dipole-dipole arrays, though extension to other configurations is straightforward. The EM-coupling component is represented as the step-current decay from a homogeneous half-space. The EM half-space response that best fits the observed data is subtracted to yield a de-coupled IP decay. Ideally, the de-coupled apparent chargeabilities are more accurate, more comparable from spread to spread, and more suitable for input to 2D and 3D inversion algorithms, e.g., Oldenburg and Li (1994), for estimation of the intrinsic chargeability distribution.

The approach is illustrated via application to dipole-dipole data from the Yilgarn Craton of Western Australia.

EM COUPLING BETWEEN PARALLEL WIRES ON A HALF-SPACE

For an infinitesimal horizontal current, Ids, oriented in the x-direction on the surface of a uniform half-space with conductivity σ, the x-component of the induced quasi-static electric field on the surface at distance r at time t after step-current shut-off is given by (Kaufman and Keller, 1983)

$$e_x(\xi, y, t) = \frac{Ids}{2\pi\sigma r^3}\left\{\mathrm{erf}(\theta r) - \frac{2}{\sqrt{\pi}}\theta r e^{-\theta^2 r^2}\right\}, \quad (1)$$

where $\xi = x - s$

$$r = \sqrt{\xi^2 + y^2}, \quad (2)$$

and

$$\theta = \sqrt{\frac{\sigma\mu_0}{4t}}. \quad (3)$$

The induced voltage recorded across a receiver dipole parallel to, but offset by distance y from, the infinitesimal electric current dipole is given by

$$v(s, y, t) = \int_a^b e_x(\xi, y, t)\,dx. \quad (4)$$

Performing the integration between points $A=(a,y)$ and $B=(b,y)$,

$$v(s, y, t) = \frac{Ids}{2\pi\sigma y^2}\left[\frac{\xi}{r}\mathrm{erf}(\theta r) - e^{-\theta^2 y^2}\,\mathrm{erf}(\theta\xi)\right]_{x=a}^{b}. \quad (5)$$

[1] Fullagar Geophysics Pty Ltd,
Level 1, 1 Swann Road,
Taringa, Qld 4068
Phone: (07) 3377 6780
Facsimile: (07) 3377 6701
E-mail: p.fullagar@mailbox.uq.edu.au

[2] CSIRO Exploration and Mining/CMTE,
PO Box 883, Kenmore, Qld 4069
Phone: (07) 3212 4630
Facsimile: (07) 3212 4455
E-mail: b.zhou@dem.csiro.au

[3] Homestake Gold of Australia Limited,
Locked Bag 12, Cloisters Square, WA 6850
Phone: (08) 9212 5813
Fax: (08) 9481 5703
E-mail: barry_bourne@homestake.com.au

For the collinear dipole case (y=0), application of L'Hopital's Rule to equation (5) yields,

$$v(s,0,t) = \frac{Ids}{4\pi\sigma}\left[(\xi^{-2} - 2\theta^2)\,\mathrm{erf}(\theta\xi) - \frac{2\theta}{\xi\sqrt{\pi}}e^{-\theta^2\xi^2}\right]_{x=a}^{b}. \qquad (6)$$

The voltage induced the receiver dipole by a finite parallel transmitter dipole is obtained by integrating equation (5) with respect to s along the length of the transmitter. Hence,

$$V(y,t) = \int_{l_1}^{l_2} v(s,y,t)ds = \frac{I}{2\pi\sigma y^2}\left[e^{-\theta^2y^2}\left[\xi\,\mathrm{erf}(\theta\xi)\right]_{\xi=x-l_1}^{x-l_2} - \left[r\,\mathrm{erf}(\theta r)\right]_{r=\sqrt{(x-l_1)^2+y^2}}^{\sqrt{(x-l_2)^2+y^2}}\right]_{x=a}^{b} \qquad (7)$$

where l_1 and l_2 are the x-coordinates of the transmitter electrodes (Figure 1). This result has been derived previously by Yost (1952).

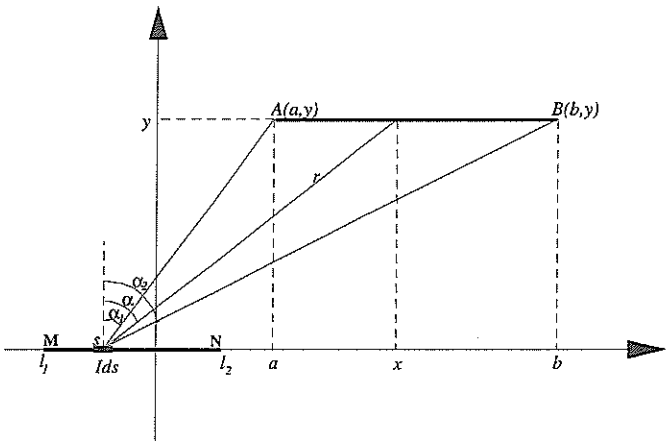

Fig. 1. Schematic system geometry, for transmitter dipole MN and receiver dipole AB on the surface of a homogeneous half-space.

Equation (7) will be suitable for pole-dipole and gradient array coupling calculations if the transmitter wire is everywhere parallel or perpendicular to the receiver dipoles, the perpendicular segments contributing nothing to the coupling. In general, it will be necessary to integrate equation (5) along the path of the transmitter wire.

At the instant of current shut-off, $\theta \to \infty$ and equation (7) reduces to

$$V(y,0+) = -\frac{I}{2\pi\sigma y^2}\left[r_{BN} - r_{BM} - r_{AN} + r_{AM}\right], \qquad (8)$$

where A,B and M,N denote the receiver and transmitter electrodes respectively (Figure 1). In general, therefore, there is no simple relationship between this induced voltage at shut-off and the DC voltage which immediately preceded it, viz.

$$V_P = \frac{I}{2\pi\sigma}\left(\frac{1}{r_{BN}} - \frac{1}{r_{BM}} - \frac{1}{r_{AN}} + \frac{1}{r_{AM}}\right). \qquad (9)$$

The formula for mutual coupling between finite collinear dipoles (y=0) follows from equation (7) by application of L'Hopital's Rule. Thus,

$$V(0,t) = \frac{-I}{2\pi\sigma}\left[\theta^2\left[\xi\,\mathrm{erf}(\theta\xi)\right]_{\xi=x-l_1}^{x-l_2} + \left[\frac{\mathrm{erf}(\theta\xi)}{2\xi} + \frac{\theta}{\sqrt{\pi}}e^{-\theta^2\xi^2}\right]_{\xi=|x-l_1|}^{|x-l_2|}\right]_{x=a}^{b} \qquad (10)$$

This is an exact expression for EM coupling between collinear dipoles on a half-space which, to the best of our knowledge, has not been published previously.

In the limit as $t \to 0$, the first term and third terms in equation (10) make no contribution to the net voltage, and the (quasi-static) induced voltage immediately after current shut-off is given by

$$V(0,0+) = -\frac{I}{4\pi\sigma}\left[\left[\frac{1}{\xi}\right]_{\xi=|x-l_1|}^{|x-l_2|}\right]_{x=a}^{b}. \qquad (11)$$

Comparing equations (11) and (9), it follows that at the instant of current shut-off the induced voltage is half the dipole-dipole DC voltage, V_P. In other words, half-space EM coupling always contributes 500mV/V to the normalised dipole-dipole response immediately after shut-off, superimposed on the desired IP signal, i.e., the V_s/V_P of Seigel (1959). This conclusion is consistent with the numerical results of Eadie (1981).

At late times, series expansion of the terms in equation (10) in the limit of small $\theta\xi$ yields

$$V|_{y=0} \to -\frac{I\theta^3}{3\pi^{3/2}\sigma}\left[\xi^2\right] \qquad \text{as } t \to \infty. \qquad (12)$$

For the dipole-dipole configuration, after evaluation of the indefinite integrals and normalisation with respect to V_P, the late-time coupling over a homogeneous half-space is approximated by

$$\hat{V}_{DD} \approx \frac{2n(n+1)(n+2)\theta^3a^3}{3\sqrt{\pi}} = \frac{n(n+1)(n+2)\mu_0^{3/2}\sigma^{3/2}a^3}{12\sqrt{\pi}}t^{-3/2} \quad \text{V/V}, \qquad (13)$$

where a is the dipole spacing. This expression is identical to that derived previously by Trofimenkoff et al. (1982).

For the pole-dipole configuration, maximum coupling will occur when all four electrodes (including the remote electrode) are collinear. In this case it follows from equation (10) that the remote electrode contributes a term $I\theta^2S/2\pi\sigma$, where S is the dipole length. This term exhibits t^{-1} time dependence, providing a strong incentive to avoid collinear remote electrodes in pole-dipole surveys.

TIME DOMAIN DE-COUPLING

De-coupling is effected here by subtracting the best-fitting EM half-space decay from the observed voltage decay. The optimal EM half-space resistivity is determined via inversion of the voltage decay, as described in the Appendix. The underlying assumption is that the EM coupling can be represented as a half-space decay, and that the residual voltage (after subtraction of the EM decay) represents the true IP response.

De-coupling via removal of an EM half-space decay can also be regarded as the first step towards spectral interpretation of the IP decay. Previous workers have modelled coupling-affected decays by introducing two Cole-Cole models, one with 'high c, low τ' to account for EM coupling, e.g., Johnson (1990). The optimal EM half-space decay is a physically more defensible choice, especially since it exhibits the appropriate limiting behaviour at early times, when coupling dominates. It may be feasible in the future to model IP decays as the superposition of an EM half-space decay and a Cole-Cole decay.

The best-fitting half-space resistivities are regarded as EM apparent resistivities. Whereas the DC resistivities are indicative of late-time behaviour, the EM apparent resistivities are early-time (high frequency limit) properties. Thus, EM apparent resistivities and DC apparent resistivities need not be identical; in practice they are qualitatively similar, but the EM apparent resistivities exhibit greater dynamic range.

The example described below refers to dipole-dipole data only. However, the de-coupling procedure can be applied to any configuration by integrating equation (5) along the transmitter wire.

DECOUPLING OF YANDAL LAGOON IP

In 1998, Homestake Gold of Australia Limited recorded 100 m dipole-dipole IP/resistivity data across an elongate north-south trending gold geochemistry anomaly at the Yandal Lagoon prospect in the north eastern part of the Yilgarn Craton, Western Australia. The data was acquired using a Scintrex IPR-12 receiver and a Scintrex TSQ-4 (10 kW) transmitter. The TSQ-4 outputs square waves with an equal on and off time period and polarity changes each half cycle. The duration of the transmitted pulse was 2 s. The received voltage windows are defined in Table 1.

The local geology and the IP survey's location are shown in Figure 2. The dolerite running north-south across the area is magnetic, and regional aeromagnetic data suggest that its western contact with the felsic sediments has been cross-cut by northeast-southwest trending fault zones. There are also numerous chlorite-rich shear zones associated with the dolerite-dacite contact north of the IP line. Both dolerite and dacite have been strongly altered, yielding chlorite, biotite, sericite and epidote. Primary mineralisation appears to be shear associated, predominantly in dolerite, locally containing up to 7% stringer and disseminated pyrite. An imperfect correlation has been observed between gold grade and pyrite content. Near-surface mineralisation was first reported in the laterite and saprolite weathering horizons. Weathering at Yandal Lagoon is typical of this part of the Yilgarn Craton: laterite 0-12 m; clays 12-40 m; saprolite 40-70 m; and bedrock from 70 m.

The dipole-dipole IP/resistivity technique was first trialed at Yandal Lagoon after petrophysical analysis confirmed that some of the primary mineralisation was chargeable. An IP anomaly was detected over a zone of increased pyritic alteration adjacent to the contact between the magnetic dolerite and the felsic sediment. The cause of the IP anomaly is interpreted to be the increase in disseminated pyrite.

LINE 8400N

Conventional apparent resistivity and EM apparent resistivity pseudo-sections for Line 8400N are presented in Figure 3. The

Window #	Width (ms)	Start (ms)	End (ms)
1-3	n/a	n/a	n/a
4	20	50	70
5	40	70	110
6	40	110	150
7	80	150	230
8	80	230	310
9	140	310	450
10	140	450	590
11	230	590	820
12	230	820	1050
13	360	1050	1410
14	360	1410	1770

Table. 1. IPR-12 voltage windows (2 s on-time)

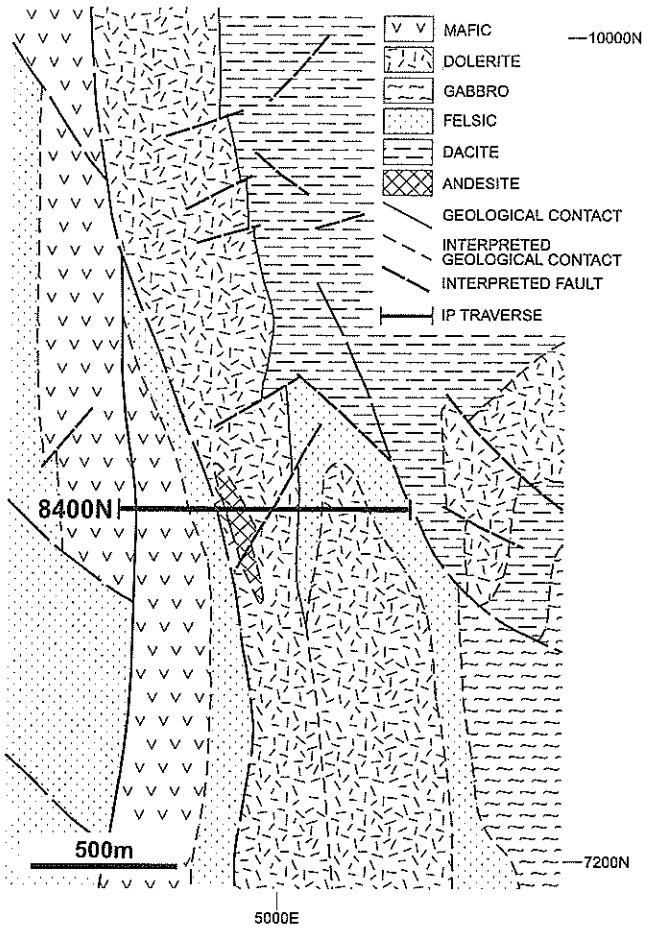

Fig. 2. Yandal Lagoon geology, and Line 8400N IP survey location.

effect of the complete bi-modal waveform was taken into account, i.e., the EM transient was modelled as the superposition of four appropriately delayed and signed step-current decays. Inversion was applied to the earliest decay window only (50-70 ms). This is reasonable, since EM effects dominate at the early times, and the signal-to-noise ratio is most favourable for the first window. A desirable consequence of computing the EM apparent conductivity from the first window alone is that the EM contribution is less than the total voltage at all later times. The variations in apparent resistivity are qualitatively very similar in Figure 3, though the EM apparent resistivity exhibits greater dynamic range.

Individual EM decays are shown in Figure 4. In Figure 4a, which corresponds to the easternmost point on the pseudo-section, the EM decay closely approximates the observed voltage at all times, implying negligible polarisation. The EM apparent resistivity is about one fifth the DC resistivity. For the station of maximum apparent chargeability in the middle of the spread, the best-fitting EM half-space decays provide a poor fit to the data at mid-late times (Figure 4b). This is clear evidence for polarisation. Two readings were taken at this station, with transmitter and receiver dipoles reversed; the agreement between the original and repeat (reciprocal) transients is only fair.

The inferences drawn from Figure 4 are borne out by the chargeability pseudo-sections in Figure 5. The upper pseudo-section is for measured chargeability over the Newmont 'Mx' window (450-1150 ms); the lower pseudo-section is the corresponding de-coupled chargeability, i.e., after subtraction of the contribution from the best fitting EM decay at each point. The difference between original and de-coupled pseudo-sections is not stark but is quite evident nonetheless: the de-coupled chargeability

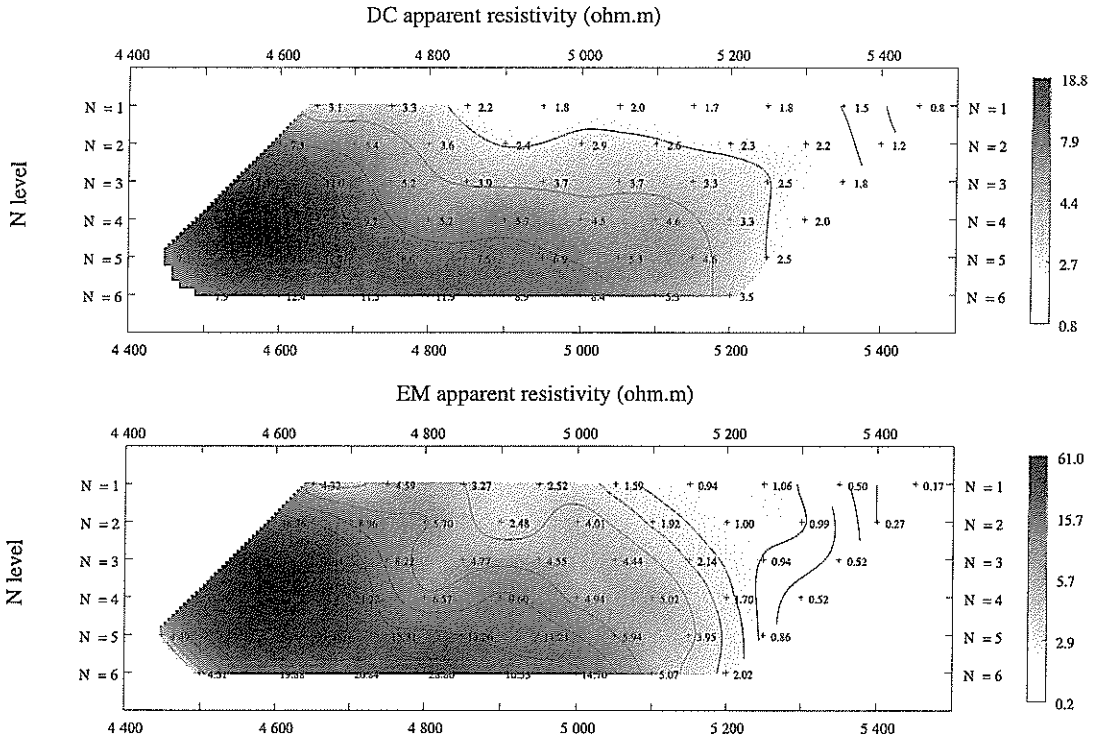

Fig. 3. Yandal Lagoon Line 8400N 100 m dipole-dipole apparent resistivity pseudo-sections, for DC (upper) and EM (50-70 ms) voltages. Logarithmic contours, 5 per decade.

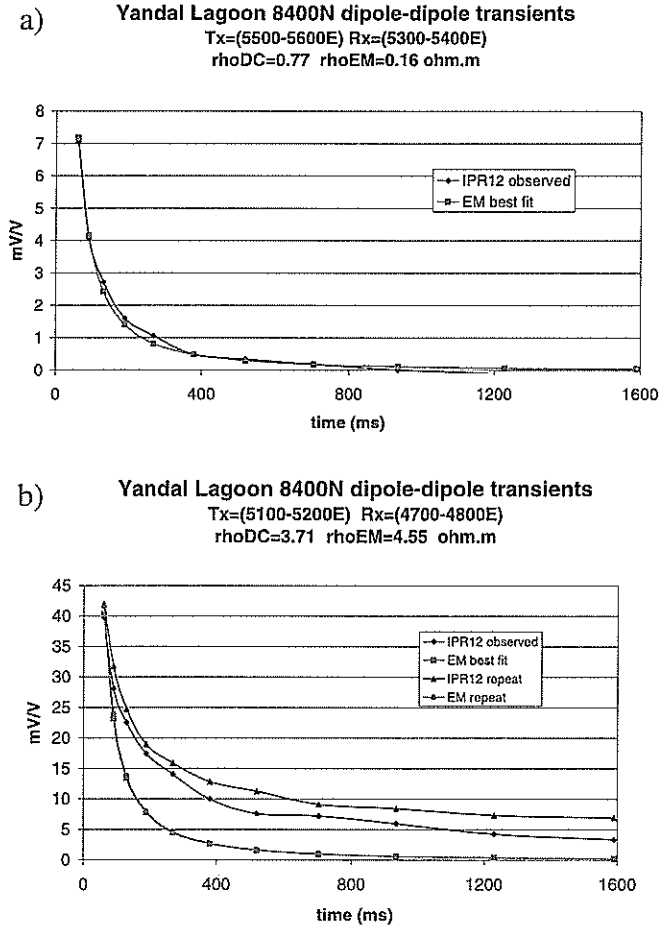

Fig. 4. Comparison of observed transients and best-fitting EM half-space decays for (a) Tx=(5500-5600E), Rx=(5300-5400E) and (b) Tx=(5100-5200E), Rx=(4700-4800E). De-coupling was performed by subtracting the EM decay from the measured transient.

is more compact, and more concentrated at shallower n-levels. Peak chargeability has decreased from 7.9 to 7.0 mV/V. Overall, the coupling corrections increase with transmitter-receiver separation (n-level) and with apparent conductivity, as they must.

CONCLUSIONS

The occurrence of significant EM coupling in IP data can compromise the exploration effectiveness of the method, by distorting both the apparent chargeabilities on pseudo-sections and the intrinsic chargeabilities predicted by 2D and 3D inversion. Moreover, coupling can thwart meaningful comparison or ranking of IP targets in hosts, or beneath cover, of differing conductivity. In addition, existence of EM coupling precludes spectral characterisation of polarisable bodies. De-coupling of frequency-domain IP is performed routinely, but in time domain surveys the coupling is normally assumed to be negligible at late times.

A fast and simple procedure has been devised for suppression of EM-coupling effects in time-domain IP data. The essence of the approach is to represent the EM coupling as a half-space decay. The half-space resistivity (EM apparent resistivity) is adjusted via inversion until the fit to the observed transient voltage decay is optimal in the least squares sense. The EM voltages associated with this best-fitting EM half-space decay are then subtracted from the measured voltages to yield a de-coupled 'IP transient'. Transients that are well represented by an EM half-space decay are deemed 'non-responsive' in the context of IP; transients that deviate markedly from an EM half-space decay are indicative of high apparent chargeability.

While de-coupling in the absence of *a priori* ground truth is necessarily approximate, this new scheme does enjoy advantages over the use of a Cole-Cole model to represent coupling: the EM component is modelled as a true EM decay, governed by a single parameter, the EM apparent conductivity.

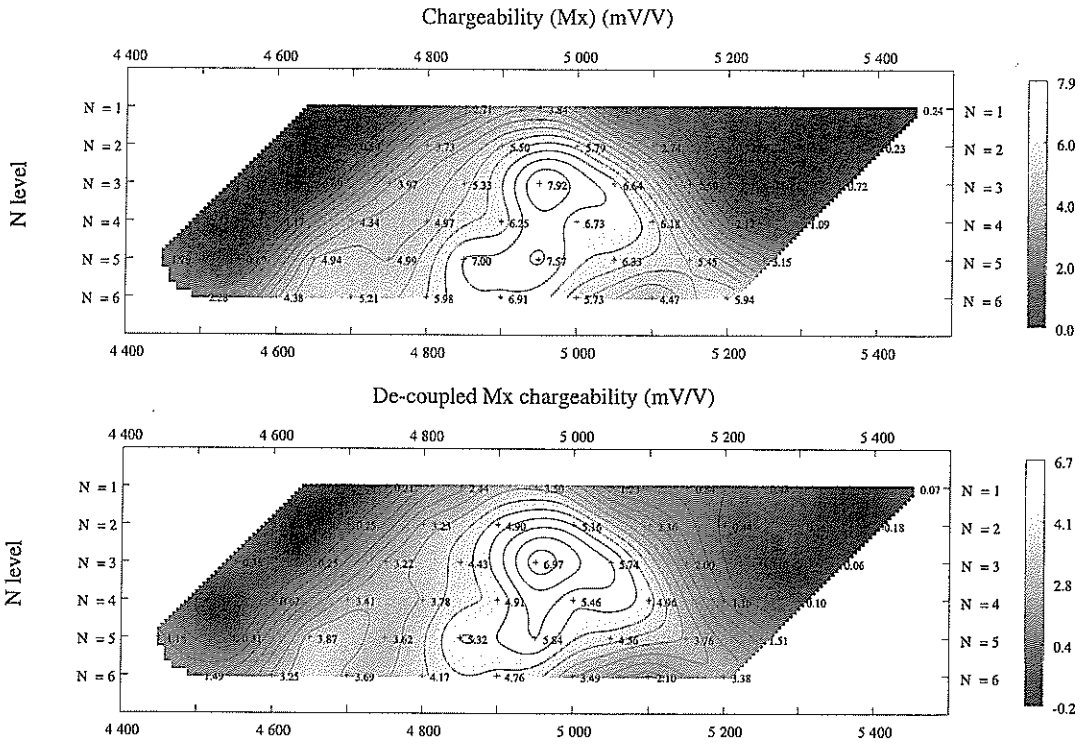

Fig. 5. Yandal Lagoon Line 8400N 100 m dipole-dipole apparent Mx chargeability pseudo-sections (450-1100 ms), for raw (upper) and de-coupled decays. Contour interval is 0.5 mV/V.

The procedure has been applied to dipole-dipole data from Yandal Lagoon, in the Yilgarn Craton of Western Australia. The decoupled chargeabilities are, necessarily, smaller than their raw counterparts, and more compact and shallower on the pseudo-sections.

The de-coupling procedure described here may expedite spectral discrimination of time-domain IP in environments with significant coupling. At present, spectral interpretation is usually based on Cole-Cole model curve matching, e.g., Seigel et al. (1997). Coupling is accounted for, if at all, as a Cole-Cole model response (Johnson, 1990). In the future, modelling the IP transient as the superposition of an EM decay and a Cole-Cole decay could prove to be an effective approach to spectral discrimination.

ACKNOWLEDGEMENTS

Data from Yandal Lagoon is published by kind permission of Homestake Gold of Australia. Todd Grant (Rio Tinto Exploration) provided important leads into the literature. We are grateful to Andre Lebel, Jim Macnae, and Mike Dentith for their constructive criticisms of the manuscript. Thanks also go to the Centre for Mining Technology and Equipment, Brisbane, for supporting this study.

REFERENCES

Coggon, J.H., 1984a, New three-point formulas for inductive coupling removal in induced polarisation: Geophysics, 49, 307-309.

Coggon, J.H., 1984b, New three-point formulas for inductive coupling removal in induced polarisation - erratum: Geophysics, 49, 1395.

Dey, A. and Morrison, H.F., 1973, Electromagnetic coupling in frequency and time-domain induced-polarization surveys over a multi-layered Earth: Geophysics, 38, 380-405.

Eadie, E.T., 1981, Detection of hydrocarbon accumulation by surface electrical methods - a feasibility study: Research in Applied Geophysics #9, Geophysics Laboratory, Univ. of Toronto.

Grant, T.W., 1990, Dipole-dipole electromagnetic coupling for 3D models: M.Sc. thesis, Univ. of Utah.

Hallof, P.G., 1974, The IP phase measurement and inductive coupling: Geophysics, 39, 650-665.

Hohmann, G.W., 1973, Electromagnetic coupling between grounded wires at the surface of a two-layer Earth: Geophysics, 38, 854-863.

Johnson, I.M., 1990, Spectral IP parameters derived from time domain measurements, in Fink, J.B., Sternberg, B.K., McAlister, E.O., Wieduwilt, W.G. and Ward, S.H., Eds., Induced Polarization - Applications and Case Histories: Society of Exploration Geophysicists, 57-78.

Kaufman, A.A. and Keller, G.V., 1983, Frequency and transient soundings: Elsevier Science Publ. Co. Inc.

Oldenburg, D.W. and Li, Y., 1994, Inversion of induced polarisation data: Geophysics, 59, 1327-1341.

Pelton, W.H., Ward, S.H., Hallof, P.G., Sill, W.R. and Nelson, P.H., 1978, Mineral discrimination and removal of EM coupling with multi-frequency IP: Geophysics, 43, 588-609.

Seigel, H.O., 1959, Mathematical formulation and type curves for induced polarisation: Geophysics, 24, 547-565.

Seigel, H.O., Vanhala, H. and Sheard, S.N., 1997, Some case histories of source discrimination using time-domain spectral IP: Geophysics, 62, 1394-1408.

Song, L., 1984, A new IP de-coupling scheme: Expl. Geophys., 15, 99-112.

Tripp, A.C., Klein, J.D., Halverson, M.O., Kingman, J. and Grant, T.W., 1990, Induced-polarization spectral interpretation including electromagnetic coupling data - a field example, in Fink, J.B., Sternberg, B.K., McAlister, E.O., Wieduwilt, W.G., and Ward, S.H., Eds., Induced Polarization - Applications and Case Histories: Society of Exploration Geophysicists, 179-198.

Trofimenkoff, F.N., Johnston, R.H. and Haslett, J.W., 1982, Electromagnetic coupling between parallel lines on a uniform earth: IEEE Trans. Geosci. and Remote Sensing, GE-20, 197-200.

Wynn, J.C. and Zonge, K.L., 1975, EM coupling - its intrinsic value, its removal, and the cultural coupling problem: Geophysics, 40, 831-850.

Yost, W.J., 1952, The interpretation of electromagnetic reflection data in geophysical exploration - Part I , General theory: Geophysics, 17, 89-106.

APPENDIX

Determination of EM apparent resistivity

In order to determine the EM apparent conductivity for each channel, it is necessary to perform a single parameter inversion. Inversion proceeds by minimising the chi-squared misfit, χ^2, defined by

$$\chi^2 = \frac{1}{N}\sum_{n=1}^{N}\frac{(o_n - c_n)^2}{\varepsilon^2} \qquad \text{(A-1)}$$

where $\{o_n: n=1,\ldots,N\}$ are the observed data, $\{c_n: n=1,\ldots,N\}$ are the corresponding calculated half-space values, and ε is the standard deviation assumed for the errors in the data. The number of data, N, contributing to the misfit is selectable; at the two extremes, the entire decay can be fitted, or just the first window. The differences between observed and calculated data are normalised with respect to ε in equation (A-1). The standard deviation is assumed identical for all windows here. If the errors in the data are realisations of independent Normal random variables with mean zero, the expected value of χ^2 is unity.

The precise definitions of the data will vary from system to system; for Scintrex IPR-12 data, as recorded at Yandal Lagoon, the data are normalised time averages of the voltage decay in mV/V, i.e.

$$o_n = \frac{1000}{V_p(t_{n+1}-t_n)}\int_{t_n}^{t_{n+1}} V(t)dt, \qquad \text{(A-2)}$$

where V_p is the steady state voltage for the Tx-Rx pair in question, and where t_n (t_{n+1}) are the start (end) times for the *nth* window.

The half-space conductivity starting value is the reciprocal of the DC apparent resistivity. At each iteration a conductivity perturbation, $\delta\sigma$, is computed, where

$$\delta\sigma = -\frac{\chi^2}{d\chi^2/d\sigma}. \qquad \text{(A-3)}$$

From (A-1), the required derivative of the misfit is given by

$$\frac{d\chi^2}{d\sigma} = -2\sum_{n=1}^{N}\frac{(o_n - c_n)}{\varepsilon^2}\frac{dc_n}{d\sigma}. \qquad \text{(A-4)}$$

The derivatives of the calculated data are computed as time integrals of derivatives of the theoretical half-space voltages, as per equation (A-2). Recalling the σ-dependence of equations (7) and (10), it is convenient to write the voltage derivatives in the form

$$\frac{dV}{d\sigma} = -\frac{V}{\sigma} + \frac{\partial V}{\partial\theta}\frac{\theta}{2\sigma}, \qquad \text{(A-5)}$$

where, from equation (3), $\partial\theta/\partial\sigma = \theta/2\sigma$. For the general offset dipole (gradient array) case, it follows from equation (7) that

$$\frac{\partial V}{\partial\theta} = -\frac{I}{\pi\sigma}\left\{\theta\xi e^{-\theta^2\gamma^2} erf(\theta\xi) + \frac{e^{-\theta^2 r^2}}{\sqrt{\pi}}\right\}. \qquad \text{(A-6)}$$

For the collinear (dipole-dipole) case, simplification of equation (A-6) or differentiation of equation (10) yields

$$\left.\frac{\partial V}{\partial\theta}\right|_{\gamma=0} = \frac{I}{\pi\sigma}\left\{\theta\xi erf(\theta\xi) + \frac{e^{-\theta^2\xi^2}}{\sqrt{\pi}}\right\}. \qquad \text{(A-7)}$$

Iterations continue until the data misfit is acceptably small ($\chi^2 < 1$), or until additional iterations do not produce any significant reduction in χ^2. The magnitude of the perturbation, $\delta\sigma$, is limited to some user-prescribed fraction of σ.